Journal of Materials Chemistry B

PAPER

View Article Online
View Journal | View Issue

Cite this: J. Mater. Chem. B, 2014, 2, 7971

Synthesis and *in vitro* evaluation of charge reversal photoresponsive quinoline tethered mesoporous silica for targeted drug delivery†

S. Karthik,[a] Avijit Jana,[b] Biswajit Saha,[d] B. Krishna Kalyani,[a] Sudip Kumar Ghosh,[d] Yanli Zhao*[bc] and N. D. Pradeep Singh*[a]

Received 16th August 2014
Accepted 1st October 2014

DOI: 10.1039/c4tb01367k

www.rsc.org/MaterialsB

We developed excellent charge reversal photoresponsive nanoparticles for targeted delivery of the anticancer drug chlorambucil. The charge reversal photoresponsive nanoparticles were constructed using two main ingredients, namely folic acid decorated mesoporous silica and quinoline chromophore. The newly synthesized quinoline chromophore performed three important roles, *i.e.*, (i) fluorescent chromophore for cell imaging, (ii) phototrigger for regulated release of anticancer drug, and (iii) charge reversal based on its zeta potential for nuclear localization. Furthermore, folic acid decorated mesoporous silica facilitated active internalization of the drug inside the cancer cells. *In vitro* biological studies reveal that our photoresponsive DDS could deliver the anticancer drug chlorambucil into the tumor cells, killing the cancer cells by both one photon (≥365 nm) and two photon (675 nm) irradiation.

Introduction

Photoresponsive nanoparticles have recently received considerable attention for their applications especially in the area of drug and gene delivery, because they allow precise control over the release, including location, timing and dosage.[1,2] In general, photoresponsive nanoparticles are composed of two main ingredients: biocompatible nanocarrier and phototrigger. A major drawback of photoresponsive nanoparticles is their non-specificity to cancer cells, which can lead to high toxicity to normal cells causing undesirable side effects. To overcome this problem, several folate-decorated photoresponsive nanoparticles have been constructed for targeted drug delivery to cancer cells.[3,4] However, these types of tumor targeted photoresponsive nanoparticles were found to be largely retained in cytoplasmic organelles, including lysosomes, rather than the nucleus of cancer cells.[5,6]

Hence, there is a real need to design multifunctional photoresponsive nanoparticles that could target not only cancer cells but the nucleus of cancer cells. They may effectively magnify the therapeutic potential of anticancer drugs.

In general, nuclear localization peptides (NLPs) and cationic polymers, such as polyethyleneimine (PEI), have been used to construct nuclear targeted photoresponsive nanoparticles.[7] Recently, pH dependent targeted charge reversal nanoparticles (TCRNs) have drawn significant attention for nuclear targeted drug delivery, because they undergo a negative to positive charge reversal when exposed to the extracellular acidic environment (pH < 7) and within the acidic lysosomal environment (pH 4–5) of cells. Because negatively charged TCRNs have some interactions with blood components, they have been used extensively *in vitro*. Shen[8] group has prepared several TCRNs that were negatively charged under neutral conditions and positively charged at endosomal pH. They have demonstrated the application of TCRNs for lysosomal pH responsive protein and gene delivery. In addition, Shen[9] and co-workers have synthesized pH responsive charge reversal polymeric micelles decorated with folic acid for both cellular and nuclear targeted drug delivery. Recently, Wang *et al.*[10] have also developed a pH responsive charge conversional nanogel for promoted tumoral cell uptake and doxorubicin delivery. Inspired by the nuclear targeted drug delivery ability of TCRNs, in this work, we developed for the first time charge reversal photoresponsive nanoparticles for both cellular and nuclear targeted delivery of anticancer drug.

The basic requirement to construct cellular and nuclear targeted charge reversal photoresponsive nanoparticles is to develop two essential ingredients: (i) chromophore that has a combination of pH sensitive charge reversal property and phototrigger ability and (ii) tumor targeted nanocarriers. For the current study, we selected quinoline moiety as a chromophore for three main reasons: (i) "quinoline derivatives are highly pH sensitive", and pK_a of quinoline is 4.8.[11] Hence, under slightly

[a]Department of Chemistry, Indian Institute of Technology, Kharagpur, India. E-mail: ndpradeep@yahoo.co.in
[b]Department of Chemistry and Biological Chemistry, Nanyang Technological University, Singapore
[c]School of Materials Science and Engineering, Nanyang Technological University, Singapore
[d]Department of Biotechnology, Indian Institute of Technology, Kharagpur, India

† Electronic supplementary information (ESI) available. See DOI: 10.1039/c4tb01367k

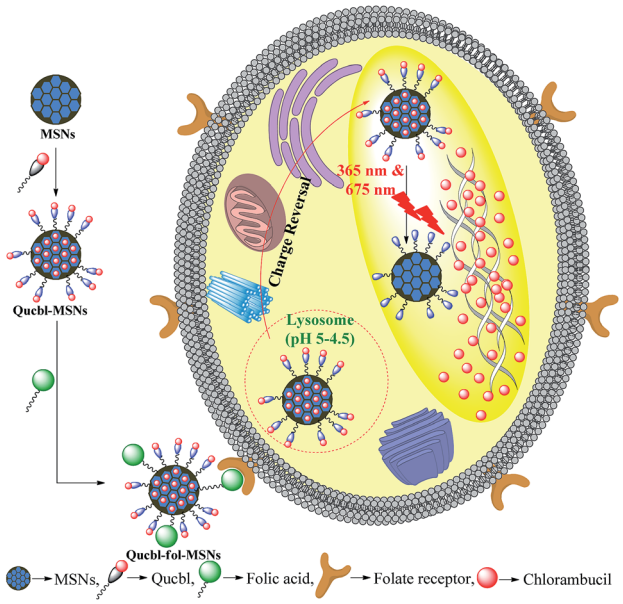

Scheme 1 Schematic illustration of the proposed tumor targeted as well as nuclear targeted delivery of anticancer drug.

acidic conditions, it can be easily protonated to reveal a positive charge, which can be exploited for charge reversal property, (ii) "quinoline-based derivatives are well known phototriggers".[12] They have been well demonstrated for the controlled release of physiologically active messengers through both one-photon excitation (1 PE) and 2 PE (near-IR light) that is the optimal wavelength for tissue penetration, and (iii) "quinoline derivatives are well known pH sensitive fluorophores", and they have been exploited for cellular imaging application. Furthermore, we also chose folic acid decorated mesoporous silica as the nanocarriers because of their biocompatibility, enhanced cellular uptake and high drug loading ability. The design of the targeted drug delivery process was schematically shown in Scheme 1.

Experimental section

Materials and methods

All reagents were purchased from Sigma Aldrich and used without further purification. Acetonitrile and dichloromethane were distilled from CaH_2 before use. ^{1}H NMR spectra were recorded on a BRUKER-AC 200 MHz spectrometer. Chemical shifts are reported in ppm from tetramethylsilane with the solvent resonance as the internal standard (deuterochloroform: 7.26 ppm). Data are reported as follows: chemical shifts, multiplicity (s = singlet, d = doublet, t = triplet, m = multiplet), coupling constant (Hz). ^{13}C NMR (50 MHz) spectra were recorded on a BRUKER-AC 200 MHz spectrometer with complete proton decoupling. Chemical shifts are reported in ppm from tetramethylsilane with the solvent resonance as the internal standard (deuterochloroform: 77.0 ppm). UV/vis absorption spectra were recorded on a Shimadzu UV-2450 UV/vis spectrophotometer, fluorescence emission spectra were recorded on a Hitachi F-7000 fluorescence spectrophotometer, FT-IR spectra were recorded on a Perkin Elmer RXI spectrometer. Transmission electron microscopy (TEM) was measured on a FEI Tecnai G220S-Twin at 200 kV. The TEM sample was prepared by dispersing compounds in water and dropping on the surface of a copper grid. Low angle powder XRD was measured by a Phillips PW 1710 X-ray diffractometer (XRD). The surface area of the mesoporous TP was measured by the N_2 sorption experiment using BET (Brunauer–Emmett–Teller) technique, performed at liquid N_2 temperature on Quantachrome Autosorb1 surface area analyzer after degassing the samples at 200 °C for 4 h. The pore size distribution curve of mesoporous TP was obtained from the analysis of the adsorption branch of the isotherm by the BJH (Barrett–Joyner–Halenda) method. The surface charge of the nanoparticles was investigated through zeta potential measurements (Zetasizer 4, Malvern Instruments, U.K.). DLS measurements at different pH were done using a Brookhaven 90 Plus particle size analyzer. Thermal analysis was done with a thermal analyzer (Pyris Diamond TG/DTA) with a heating rate 8 °C min^{-1} in a temperature range 50 to 1000 °C. Photolysis of the ester conjugate was carried out using a 125 W medium pressure Hg lamp supplied by SAIC (India) and laser diode of 675 nm, 15 mW supplied by Thor Labs. Chromatographic purification was done with 60–120 mesh silica gel (Merck). For reaction monitoring, pre-coated silica gel 60 F254 TLC sheets (Merck) were used. RP-HPLC was taken using mobile phase acetonitrile, at a flow rate of 1 mL min^{-1} (detection: UV 254 nm). Cell imaging was done with an Olympus confocal microscope (FV1000, Olympus) using the respective filter.

Synthesis of Qucbl. Quinoline chlorambucil conjugate (Qucbl) was synthesized using a previously reported procedure (ESI Scheme S1†).[13]

Synthesis of trimethoxysilyl tagged Qucbl. Amino propyl trimethoxy silane (0.5 mL) was added to an ice-cooled solution of compound 1 (150 mg) in dry DCM (10 mL). After stirring for 6 h, the solvent was removed by rotary evaporation to yield 175 mg of trimethoxysilyl tagged Qucbl, which was used in the next step without purification.

Synthesis of quinoline chlorambucil loaded on MSNs Q1 (Qucbl-MSNs). Trimethoxysilyl tagged Qucbl was dissolved in dry toluene (10 mL) containing 100 mg of mesoporous silica nanoparticles and the mixture was refluxed for 20 h at 80 °C to afford compound Q1(Qucbl-MSN). The course of loading was followed by UV-vis absorption spectra for a regular time interval. Finally the materials were recovered by centrifugation, washed twice with toluene and dried under vacuum. We calculated Qucbl loaded on mesoporous silica nanoparticle using the equation below:

$$\text{Quinoline chlorambucil loaded on MSNs} = \frac{(\text{Initial conc. of Qucbl} - \text{final conc. of Qucbl in reaction medium}) \times \text{M. wt of Qucbl}}{\text{Amount of mesoporous silica taken}}$$

Synthesis of folate loaded Qucbl-MSNs Q2 (Qucbl-Fol-MSNs).[13] Folic acid was attached to Qucbl-MSNs. In a round bottom flask, folic acid (50 mg) and APTS (0.2 mL) were mixed in DMSO (3 mL). *N*-Hydroxysuccinimide (30 mg) and 1-(3-dimethylaminopropyl)-3-ethylcarbodiimide hydrochloride (50 mg) were then added into the mixture and stirred for 2 h. To the reaction mixture, 50 mg of Q1 DMSO suspension was added and the mixture was stirred for 20 h at room temperature. The MSN have approximately 0.5 wt% of folic acid grafted on the surface of Q1. Finally, folate decorated quinoline chlorambucil tagged MSN Q2 (Qucbl-Fol-MSN) was recovered by centrifugation, washed twice with toluene and dried under vacuum.

Hydrolytic stability of Q2. To check the stability of Q2 in the cell culture medium, we dispersed 1 mg mL^{-1} Q2 with 10% fetal bovine serum and incubated at 37 °C in the dark for 72 h. The tubes were kept in an ultrasonic bath for 10 min to make the solutions homogeneous and stored at 37 °C in dark condition for 96 h. Then all the solutions were centrifuged (5000 rpm) for 10 min and the supernatant solutions were analyzed by reverse phase HPLC to examine the percentage of drug depleted.

Cell imaging and cytotoxicity of MSNs, and Q2 on HeLa cell line

Qucbl-Fol-MSNs for cell imaging studies using HeLa cell line. Cell imaging studies were carried out using the HeLa cell line, which was maintained in minimum essential medium (MEM) containing 10% fetal bovine serum (FBS) at 37 °C and 5% CO_2. To study the cellular uptake of Q2, HeLa cells (5×10^4 cells per well) were plated on 12 well plates and allowed to adhere for 4–8 hours. Cells were then incubated with 50 μg of Q2 separately in cell culture medium for 4 h at 37 °C in 5% CO_2. Thereafter, cells were fixed in paraformaldehyde for 15 min and washed two times with PBS. Imaging was done with an Olympus confocal microscope (FV1000, Olympus) using the respective filter.

Lyso tracking experiment. Cell imaging studies were carried out using the HeLa cell line, which was maintained in Dulbecco's Modified Eagle Medium (DMEM) containing 10% fetal bovine serum (FBS) at 37 °C in 5% CO_2. To study the intracellular localization of Q2 nanoparticles, briefly HeLa cells (5×10^4 cells per well) were plated on coverslips in 6 well plates and allowed to adhere for 4–8 hours. Cells were then incubated with 50 μg of Q2 in PBS for 6 h at 37 °C in 5% CO_2. Then, the medium was discarded and the cells were washed two times with PBS followed by the addition of LysoTracker Red DND-99 (2 mL, 50 nM) in culture medium and incubated at 37 °C in 5% CO_2 for 1 h. Thereafter, cells were fixed in paraformaldehyde for 15 min and washed two times with PBS. Imaging was done with a Nikon confocal microscope (Nikon Eclipse TE2000-E) using the respective filter.

Time dependent internalization studies of Q2 at pH 7.4. Following the above procedure HeLa cells (5×10^4 cells per well) were plated on coverslips in 6-well cell culture plates and allowed to adhere for 4–8 hours. Cells were then incubated with 50 μg of Q2 in PBS for different time intervals at 37 °C in 5% CO_2. Thereafter, cells were fixed in paraformaldehyde for 15 min and washed two times with PBS. Imaging was done with a Nikon confocal microscope (Nikon Eclipse TE2000-E) using the respective filter.

Time dependent internalization studies of Q2 at pH 7.4. We followed the same procedure except the Qucbl-Fol-MSN nanoparticles were dispersed in PBS of pH 4.8.

Nuclear co-localization studies using Qucbl-Fol-MSNs and a nuclear staining dye propidium iodide. Cells, grown and plated as described above, were incubated for 4 h at 37 °C with 1 mL of MEM containing 20 μM of Qucbl-Fol-MSNs. Thereafter, cells were washed 3 times with 10 mM PBS and fixed with 2% paraformaldehyde for 15 min at room temperature. After fixation cells were washed 3 times with 10 mM PBS permeabilized with 0.01% Triton X 100, a non-ionic surfactant. The cells were counterstained with 10 μg mL^{-1} propidium iodide (PI) and 0.5 μg mL^{-1} RNASE at room temperature in the dark for 30 min. After gentle washing in 10 mM PBS for 3 times, the cells were viewed under a confocal microscope.

Photolysis of Q2 using soft UV irradiation (≥365 nm) and 675 nm laser diode

Photolysis of Q2 using soft UV irradiation (≥365 nm). A suspension of 5 mg/5 mL of the Q2 was prepared in acetonitrile. Half of the suspension was kept in dark and to the remaining half nitrogen was passed and irradiated using a 125 W medium pressure Hg lamp as the light source ($\lambda \geq 365$ nm) and 1 M $CuSO_4$ solution in 0.1 N H_2SO_4; the transmittance for the above filter = 365 to 500 nm. At regular time intervals, a small aliquot (100 μL) of the suspension was taken out and centrifuged (5000 rpm) for 10 min; the obtained transparent solution was analyzed by reverse phase HPLC using mobile phase acetonitrile at a flow rate of 1 mL min^{-1}.

Photolysis of Q2 using red laser. 1 mg of Q2 was dissolved in 1 ml acetonitrile. Half of the solution was kept in dark and to the remaining half nitrogen was passed and irradiated using a 675 nm laser diode (15 mW cm^{-2}). At regular time intervals, a small aliquot (100 μL) of the suspension was taken out and centrifuged (5000 rpm) for 10 min; the obtained transparent solution was analyzed by reverse phase HPLC using mobile phase acetonitrile at a flow rate of 1 mL min^{-1}.

Cytotoxicity of Q1 and Q2 on HeLa cell line

Cytotoxicity before photolysis. The cytotoxicity *in vitro* was measured using the MTT (3-(4,5-dimethylthiazol-2-yl)-2,5-diphenyltetrazolium bromide, a yellow tetrazole) assay on HeLa cell line. Briefly, cells growing in log phase were seeded into 96-well cell-culture plate at 1×10^4 cells per mL. Different concentrations of Q1, Q2 and chlorambucil were added in the wells with an equal volume of PBS in the control wells. The cells were then incubated for 72 h at 37 °C in 5% CO_2. Thereafter, fresh media containing 0.40 mg mL^{-1} MTT were added to the 95 well plates and incubated for 4 h at 37 °C in 5% CO_2. Formazan crystals thus formed were dissolved in DMSO after decanting the earlier media and absorbance recorded at 595 nm.

Cytotoxicity after photolysis. HeLa cells maintained in minimum essential medium (in 96-well cell-culture plate at

concentration of 1×10^4 cells per mL) containing 10% fetal bovine serum (FBS) and different concentrations of Q1, Q2 and chlorambucil were incubated for 4 h at 37 °C in 5% CO_2. Then the cells were irradiated (keeping the cell-culture plate 5 cm apart from the light source) using a 125 W medium pressure Hg lamp as irradiation source (≥365 nm) and 1 M $CuSO_4$ solution as UV cut-off filter. After irradiation the cells were again incubated for 72 h. Then cytotoxicity was measured using the MTT assay as described in the earlier section.

Results and discussion

We synthesized mesoporous silica nanoparticles (MSNs) using a previously reported procedure.[13a] Transmission electron microscopy (TEM), powder X-ray diffraction and nitrogen sorption isotherm analysis reveals that MSNs are of ~50–66 nm particle size, and have a honeycomb like porous structure with a 2.9 nm average pore diameter and a surface area of 302.69 m^2 g^{-1} (ESI, Fig. S1–S3†). Subsequently, quinoline chlorambucil conjugate (Qucbl) was synthesized using a previously reported procedure[13b] (Scheme S1†). Finally, Qucbl and folic acid were covalently anchored on the surface of MSNs with silane coupling agent in a stepwise manner as depicted in Scheme 2. Quinoline-chlorambucil loaded mesoporous silica Q1 (Qucbl-MSNs) and folic acid decorated quinoline-chlorambucil loaded mesoporous silica Q2 (Qucbl-Fol-MSNs) were characterized by IR spectra, solid state UV and thermogravimetric analysis (TGA) (Fig. S4–S6†).

The physicochemical properties of Q2 such as morphology, size, and zeta potential were studied because they have influence on cellular uptake. DLS (Fig. S7†) studies reveal that the average particle size of MSNs, Q1 and Q2 were 85.26 ± 1.82 nm, 134.82 ± 1.54 nm and 143.49 ± 1.52 nm, respectively. The increase in particle size of Q2 compared to free MSNs and Q1 implies that mesoporous silica was decorated by both folic acid and Qucbl conjugate. TEM observation shows that MSNs, Q1 and Q2 were well dispersed and spherical in shape. The size of the Q2 is well within the preferred range of the nanoparticles useful for effective drug delivery.

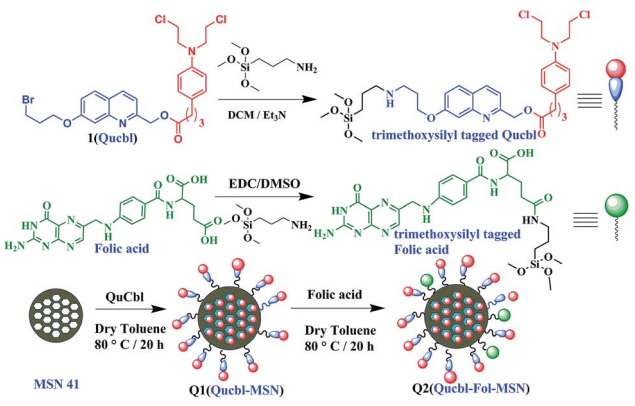

Scheme 2 Synthesis of quinoline-chlorambucil loaded mesoporous silica (Qucbl-MSNs) and quinoline chlorambucil and folic acid decorated mesoporous silica (Qucbl-Fol-MSNs).

The amount of the quinoline chlorambucil loaded on MSNs is calculated to be about ~273 μg mg^{-1}, based on UV-Vis absorption spectra (Fig. 1). The UV-Vis absorption and fluorescence spectra of Q2 are presented in Fig. S8.† Similar to quinoline chromophore, Q2 also showed broad absorbance from 300 to 365 nm and emission maxima at 460 nm. Hence, Q2 can be explored like quinoline chromophore for simultaneous cell imaging and release of the anticancer drug by both one photon (365 nm) and two photon (675 nm) excitation.

A key pH dependent charge reversal property of Q1 and Q2 was determined by measuring their zeta potentials at different acidities (Fig. 2a). The MSNs revealed a zeta potential of about −19 mV in acidic pH ranges of 6.5–3, indicating that they always remain negatively charged due to the presence of Si–OH group on their surface. On the other hand, Q1 and Q2 showed zeta potentials of −5 mV and −1 mV at pH 6.5, respectively. But, in the pH ranges of 5–4.5, both Q1 and Q2 became positively charged, and gradually, their zeta potential reached about +1.65 mV and +3.67 mV, respectively. At pH 3, the zeta potentials of Q1 and Q2 were found to be about +9.5 mV and +11.6 mV, respectively.

To evaluate the proton-binding behaviour of Q2, we recorded the emission spectra of model compound **2** in Na_2HPO_4–citrate buffer at different pH values ranging from 7.0 to 2.6 (Fig. 2b). We noted the fluorescence maxima of compound **2** in neutral pH is around 380 nm, which was red shifted to 450 nm at lower pH. Interestingly, we also observed an isoemissive point in emission spectra at around 410 nm, indicating the presence of two distinct species in equilibrium. This is because, at lower pH, protonation is favoured and hence protonated **2** is the predominant species. Further proton-binding behavior of compound **2** was also supported by ^{1}H NMR spectroscopy. We recorded ^{1}H NMR spectrum of compound **2** and its protonated form (10 mM HCl). As shown in Fig. 1c, on protonation, the quinolinic protons H3 and H4 displayed significant downfield shifts to 8.99 and 8.25 ppm respectively, suggesting that the protonation occurred at the quinolinic site.

On the other hand, we explored the pH dependent charge reversal properties of Q2 *in vitro* by carrying out cellular internalization studies at two different pH, 7.4 and 4.8.[8,9] The time dependent confocal laser scanning microscopy (CLSM) imaging studies showed a significant difference in cellular internalization of Q2 at pH 7.4 and 4.8. At pH 4.8, Q2 were more effectively

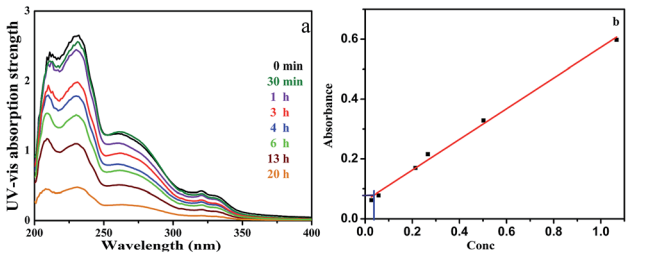

Fig. 1 Quinoline chlorambucil loaded on MSNs. (a) The course of loading was followed by UV-vis absorption spectra; (b) calibration curve for the concentration of chlorambucil on the surface of MSNs.

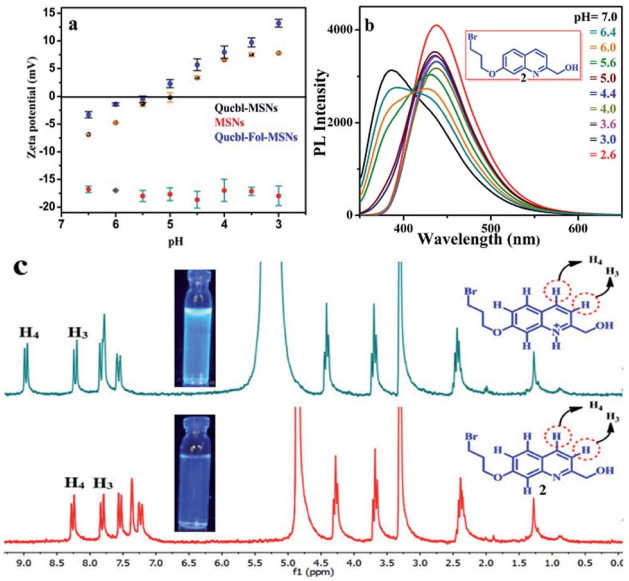

Fig. 2 (a) The zeta potential of MSNs, Qucbl-MSNs (Q1) and Qucbl-Fol-MSNs (Q2) at different pH. (b) pH responsive fluorescence spectra of compound **2**. (c) ^{1}H NMR spectra of compound **2** in 10 mM HCl (10 μL) in MeOH-D4 (inset of (c): corresponding emission images from protonated and non-protonated **2** under UV light of 366 nm).

internalized by the cell membrane (Fig. S9†) than that at pH 7.4. The above mentioned studies clearly indicate that Q2 is indeed charge-reversal nanoparticles. Thus, Q2 should be negatively charged at physiological pH and be suitable for *in vivo* applications. Once localized in solid tumors/lysosomes, Q2 will undergo negative to positive charge reversal and thus be more readily internalized by the cells. Further, the effectiveness of the targeting group folic acid on the Q2 in binding folate receptors and promoting the cellular uptake was evaluated using HeLa cells and normal cells-L929, because it is well known that folate receptors are over-expressed in HeLa cells compared to normal cells.[14] The time dependent CLSM imaging studies (0–6 h) revealed that Q2 was internalized to a greater extent in HeLa cells compared to normal cells-L929 (Fig. 3).

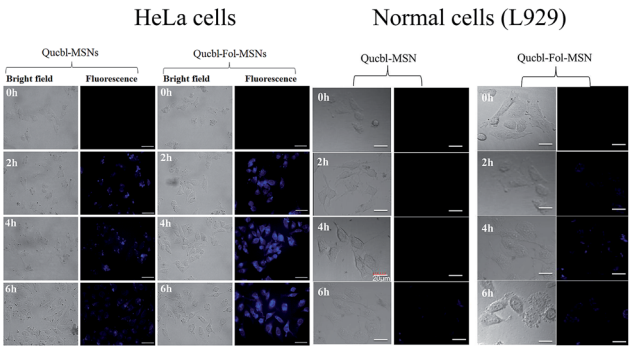

Fig. 3 Time dependent CLSM images of HeLa cells and normal cell (L929) incubated with of Qucbl-Fol-MSNs (Q2) and Qucbl-MSNs (Q1) (without folic acid) for 6 h. The blue fluorescence is from the Qucbl conjugate of the MSNs. Scale bar: 20 μm.

Furthermore, the above mentioned studies also showed that Q2 was largely internalized in HeLa cells compared to Q1. The intracellular distribution of Q2 was further evaluated by CLSM. A LysoTracker Red dye DND-99 was used to stain the acidic organelles in HeLa cells. We found that Q2 were dominantly localized in LysoTracker-labeled acidic organelles after 6 h of incubation (Fig. 4a–d). Those nanoparticles that were trapped inside endosomes/lysosomes are pink in color. Nevertheless, some of the Q2 appeared to be able to escape from the endosome, and was distributed in the cytoplasm. The nitrogen of the quinoline unit on the nanoparticles was protonated at acidic endosomal pH, which could disrupt the endosome and promote the escape of the nanoparticles from the endosome into the cytoplasm. The behaviour can be attributed to the "proton-sponge" or "endosome buffering" effect.[13a]

We also investigated the nuclear localization ability of Q2. Previous literature studies indicated that nuclear localization of TCRNs was observed after longer time of incubation (20–24 h).[15,16] Hence we incubated HeLa cells with Q2 for 24 h. To distinguish, nuclei were stained with PI, showing red fluorescence in the images. Fig. 4g showed strong fluorescence corresponding to Q2, which was quite evenly distributed throughout the cytoplasm and nucleus, indicating that the drug might have entered into the nucleus. In general, nanoparticles larger than 70 nm in diameter were considered to be quite large to enter into cell nuclei. Our newly synthesised nanoparticles Q2 have an average particle size of 143.49 nm. Hence, we presume that our photocage compound Qucbl would have been leached out from silica cores of Q2 due to the breakage of secondary silica coating in acidic medium, and then, freely diffused throughout the whole intracellular area, resulting in the accumulation of Qucbl

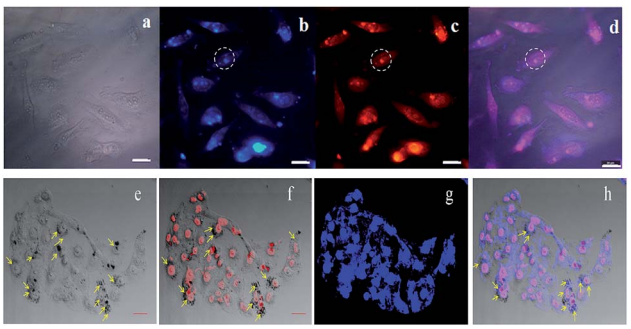

Fig. 4 Confocal fluorescence images of HeLa cells: (a and e) bright field images of cells that were incubated with 50 μg Qucbl-Fol-MSNs (Q2) for 6 h, (b and g) showing the uptake of Qucbl-Fol-MSNs (Q2) (λ_{ex} = 365 nm), (c) emission from LysoTracker Red DND-99 (25 nM, λ_{ex} = 535 nm), (d) fluorescent and bright field overlay image of (b) and (c) showing both Qucbl-Fol-MSNs (Q2) and DND-99 were located at the lysosome. The blue fluorescence is from Qucbl-Fol-MSNs (Q2) and the red fluorescence is from red dye DND-99 used to stain the lysosome, (f) showing the uptake of PI (propidium iodide) (25 nM, λ_{ex} = 535 nm), (h) fluorescent and bright field overlay image of (f) and (g) showing that both Qucbl-Fol-MSNs (Q2) and PI were located at the cell nuclei. The blue fluorescence is from Qucbl-Fol-MSNs (Q2) and the red fluorescence is from PI used to stain the nuclei (scale bar = 20 μm (a–d) and 30 μm (e–h)).

in the nucleus due to its intercalation with double stranded DNA.[17]

After successful demonstration of cellular internalization and distribution of Q2, we studied photoinduced anticancer drug release behaviour of Q2. The time courses of the anticancer drug release by Q2 under photolysis at both ≥365 nm (Hg vapour lamp) and two-photon 675 nm diode laser were monitored by HPLC. The HPLC profile indicates (Fig. 5a) that, after 45 min of irradiation, 65% of loaded anticancer drug (chlorambucil) was effectively released by using UV light ($\lambda \geq$ 365 nm, 120 mW cm^{-2}), whereas 15% of the drug was released using the diode laser (675 nm, 15 mW cm^{-2}) (Fig. S10†), suggesting that external light intensity could regulate the drug release. Furthermore, we demonstrated precise control over the photolytic release of loaded anticancer drug by monitoring the release of chlorambucil after periods of exposure to light and dark conditions (Fig. 5b), which clearly showed that the drug release proceeded only under illumination. In addition, the photochemical quantum yield of Q2 was measured to be 0.29, which resembles a previous report.[12]

After successful demonstration of photoinduced anticancer drug release by Q2, we evaluated the cytotoxicity of chlorambucil, Q2, and MSNs *in vitro* using the MTT assay in HeLa cell line. It was observed that cell viability remains above 90% at 50 μg mL^{-1} of Q2 and MSNs. However, cells treated with chlorambucil showed increasing cytotoxicity with increasing drug concentration (Fig. 6a). The above mentioned studies indicated that Q2 and MSNs were relatively nontoxic to the cells. For the light exposure experiment, cells incubated with chlorambucil, Q2, and MSNs were irradiated for 30 min under UV light (≥365 nm). Cell viability of 27.8% was observed with free chlorambucil at the concentration of 50 μg mL^{-1}. For the same concentration of Q2, the cell viability of 23% was noted, which can be due to the efficient photorelease of anticancer drug chlorambucil inside the cancerous cell. Further, 73% cell viability was observed at the concentration of 50 μg mL^{-1} for two photon irradiation (Fig. S11†). On the other hand, cell viability was found to be largely unaffected by drug-free MSNs, indicating the cytotoxicity was likely caused by the released drug chlorambucil upon light irradiation on Q2. In comparison with the same concentration of chlorambucil to that of Q2 (Fig. 6b), Q2 showed much lower cytotoxicity. But upon irradiation, Q2 showed an enhanced cytotoxicity to cancer cells in comparison to chlorambucil because of the efficient photorelease of chlorambucil inside the cancerous cells.

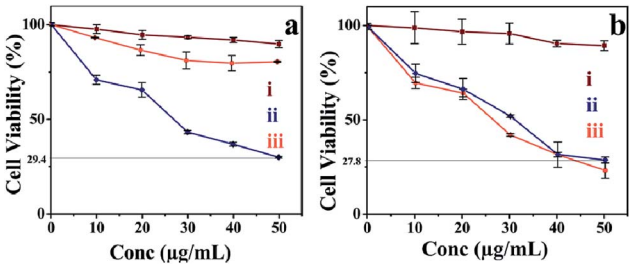

Fig. 6 (a–b) Cell viability test of (i) MSNs, (ii) chlorambucil, and (iii) Qucbl-Fol-MSNs (Q2) and in HeLa cell line: (a) before irradiation and (b) after irradiation. Values are presented as mean ± SD.

Conclusion

We have developed pH dependent charge reversal photoresponsive nanoparticles for *in vitro* targeted drug delivery. The TCRNs, *i.e.*, Qucbl-Fol-MSNs, were negatively charged in neutral solution and quickly transformed into positively charged at pH 6 and highly positively charged at pH 5.0–4.5. The charge reversal has enhanced the cellular uptake of the photoresponsive TCRNs and greater accumulation of drug in the nucleus and cytoplasm. Even though the size of the nanoparticle was much larger than that of nuclear pores, the released Qucbl from the silica cores was able to freely diffuse and accumulated inside the nucleus, giving much improved cytotoxicity. Photoregulated drug release ability of Qucbl-Fol-MSNs has been established by means of periodic exposure to light and dark conditions. Strong fluorescence of Qucbl-Fol-MSNs has been explored for the *in vitro* cellular imaging application and precise drug release inside the cancer cells upon irradiation. Thus, we expect that the above mentioned study may be a promising starting point for the utilization of charge reversal photoresponsive nanoparticles in construction of nuclear targeted drug delivery systems.

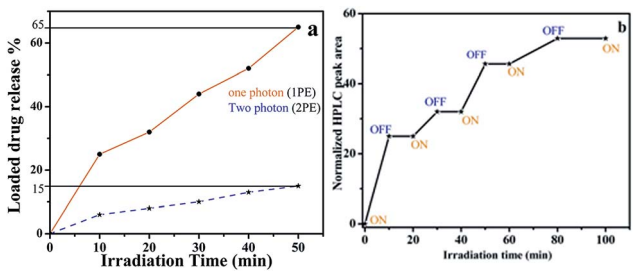

Fig. 5 (a) Time course for the photorelease of chlorambucil from Qucbl-Fol-MSNs (Q2) under soft UV irradiation 1 PE (≥365 nm, 120 mW cm^{-2}) and 2 PE (675 nm, 15 mW cm^{-2}). (b) Progress of release of chlorambucil under bright and dark conditions. "ON" indicates the beginning of light irradiation and "OFF" indicates the ending of light irradiation.

Acknowledgements

DST-SERB for financial support. DST-FIST for 400 MHz NMR and CLSM. S. Karthik is thankful to IIT KGP, B. Krishna Kalyani to Inspire Fellowship and Biswajit Saha to DBT for their fellowship. Yanli Zhao thanks financial support from the Singapore National Research Foundation Fellowship (NRF2009NRFRF001-015).

Notes and references

1 M. S. Yavuz, Y. Cheng, J. Chen, C. M. Cobley, Q. Zhang, M. Rycenga, J. Xie, C. Kim, K. H. Song, A. G. Schwartz, L. V. Wang and Y. Xia, *Nat. Mater.*, 2009, **8**, 935.

2 T. M. Allen and P. R. Cullis, *Science.*, 2004, **303**, 1818.
3 (*a*) H. Meng, M. Xue, T. Xia, Y. L. Xia, Y. Zhao, F. Tamansoi, J. F. Stoddart, J. I. Zink and A. E. Nel, *J. Am. Chem. Soc.*, 2010, **132**, 12690; (*b*) Y. Zhu and M. Fujiwara, *Angew. Chem., Int. Ed.*, 2007, **46**, 2241.
4 (*a*) S. Angelos, Y. Yang, N. M. Khashab, J. F. Stoddart and J. I. Zink, *J. Am. Chem. Soc.*, 2009, **131**, 11344; (*b*) N. K. Mal, M. Fujiwara and Y. Tanaka, *Nature*, 2003, **421**, 350; (*c*) E. J. L. Vivero, I. I. Slowing, C. Wu and V. S. Y. Lin, *J. Am. Chem. Soc.*, 2009, **131**, 3462; (*d*) S. A. Mackowiak, A. Schmidt, V. Weiss, C. Argyo, C. V. Schirnding, T. Bein and C. Brauchle, *Nano Lett.*, 2013, **13**, 2576.
5 (*a*) J. Babin, M. Pelletier, M. Lepage, J. Allard, D. Morris and Y. Zhao, *Angew. Chem., Int. Ed.*, 2009, **48**, 3329; (*b*) C. Park, J. Lim, M. Yun and C. Kim, *Angew. Chem., Int. Ed.*, 2008, **47**, 2959; (*c*) Q. Lin, Q. Huang, C. Li, C. Bao, Z. Liu, F. Li and Z. Linyong, *J. Am. Chem. Soc.*, 2010, **132**, 10645.
6 (*a*) F. Porta, G. E. M. Lamers, J. Morrhayim, A. Chatzopoulou, M. Schaaf, H. Dulk, C. Backendorf, J. I. Zink and A. Kros, *Adv. Healthcare Mater.*, 2013, **2**, 281; (*b*) Y. Yang, B. Velmurugan, X. Liu and B. Xing, *Small*, 2013, **17**, 2937.
7 (*a*) N.-C. Cheng, F.-Y. Annie Ho and C.-S. Yeh, *Angew. Chem., Int. Ed.*, 2012, **51**, 8806; (*b*) D. Mandal, A. N. Shirazi and K. Parang, *Angew. Chem., Int. Ed.*, 2011, **50**, 9633; (*c*) L. Pan, Q. He, J. Liu, Y. Chen, M. Ma, L. Zhang and J. Shi, *J. Am. Chem. Soc.*, 2012, **134**, 5722; (*d*) V. P. Torchilin, *Adv. Drug Delivery Rev.*, 2008, **60**, 548.
8 Z. Zhou, Y. Shen, J. Tang, E. Jin, X. M. Q. Sun, B. Zhang, E. A. Van Kirk and W. J. Murdoch, *J. Mater. Chem.*, 2011, **21**, 19114.
9 P. Xu, K. E. A. Van, Y. Zhan, W. J. Murdoch, M. Radosz and Y. Shen, *Angew. Chem., Int. Ed.*, 2007, **46**, 4999.
10 J.-Z. Du, T.-M. Sun, W.-J. Song, J. Wu and J. Wang, *Angew. Chem., Int. Ed.*, 2010, **49**, 3621.
11 J. Clark and D. D. Perrin, *Q. Rev., Chem. Soc.*, 1964, **18**, 295.
12 (*a*) Y. Zhu, C. M. Pavlos, J. P. Toscano and T. M. Dore, *J. Am. Chem. Soc.*, 2006, **128**, 4267; (*b*) M. J. Davis, C. H. Kragor, K. G. Reddie, H. C. Wilson, Y. Zhu and T. M. Dore, *J. Org. Chem.*, 2009, **74**, 1721.
13 (*a*) Q. Zhang, F. Liu, K. T. Nguyen, X. Ma, X. Wang, B. Xing and Y. Zhao, *Adv. Funct. Mater.*, 2012, **22**, 5144; (*b*) S. Karthik, B. Saha, S. K. Ghosh and N. D. P. Singh, *Chem. Commun.*, 2013, **49**, 10471.
14 (*a*) A. Agostini, L. Mondragón, A. Bernardos, R. Martínez-Máñez, M. Dolores Marcos, F. Sancenón, J. Soto, A. Costero, C. Manguan-García, R. Perona, M. Moreno-Torres, R. Aparicio-Sanchis and J. R. Murguía, *Angew. Chem., Int. Ed.*, 2012, **51**, 10556; (*b*) I. Slowing, B. G. Trewyn and V. S.-Y. Lin, *J. Am. Chem. Soc.*, 2006, **128**, 14792.
15 (*a*) Z. Chu, S. Zhang, B. Zhang, C. Zhang, C.-Y. Fang, I. Rehor, P. Cigler, H.-C. Chang, G. Lin, R. Liu and Q. Li, *Sci. Rep.*, 2014, **4**, 4495; (*b*) H. L. Kim, S. B. Lee, H. J. Jeong and D. W. Kim, *RSC Adv.*, 2014, **4**, 31318.
16 H. Jang, S.-R. Ryoo, K. Kostarelos, S. W. Han and D.-H. Min, *Biomaterials*, 2013, **34**, 3503.
17 J. Zhao, W. Li, R. Ma, S. Chen, S. Ren and T. Jiang, *Int. J. Mol. Sci.*, 2013, **14**, 16851.